Polymer Chemistry

ROYAL SOCIETY OF CHEMISTRY

PAPER

View Article Online
View Journal | View Issue

Cite this: *Polym. Chem.*, 2022, **13**, 655

RAFT aqueous dispersion polymerization of 4-hydroxybutyl acrylate: effect of end-group ionization on the formation and colloidal stability of sterically-stabilized diblock copolymer nanoparticles†

Deborah L. Beattie, Oliver J. Deane, Oleksandr O. Mykhaylyk and Steven P. Armes *

A series of all-acrylic poly(2-hydroxyethyl acrylate)$_x$-poly(4-hydroxybutyl acrylate)$_y$ (PHEA$_x$–PHBA$_y$) diblock copolymer nanoparticles were prepared *via* an efficient one-pot RAFT aqueous dispersion polymerization protocol using either a carboxylic acid-functionalized RAFT agent (HOOC–PHEA$_x$–PHBA$_y$) or a morpholine-functionalized RAFT agent (Mo–PHEA$_x$–PHBA$_y$). The pH-dependent colloidal stability of the resulting sterically-stabilized nanoparticles was assessed by dynamic light scattering (DLS) and aqueous electrophoresis. The HOOC–PHEA$_{73}$–PHBA$_{217}$ nanoparticles exhibited reversible flocculation below pH 5.1, whereas the Mo–PHEA$_{76}$–PHBA$_{160}$ nanoparticles flocculated above pH 5. Moreover, the HOOC–PHEA$_{73}$–PHBA$_{217}$ nanoparticles proved to be sensitive to added salt, with incipient flocculation occurring in the presence of 20–60 mM KCl owing to charge screening. Thus, such nanoparticles require end-group ionization to confer colloidal stability *via electrosteric* stabilization. However, reducing the PHBA/PHEA molar ratio and/or increasing the PHEA$_x$ stabilizer DP, leads to more efficient steric stabilization and hence enhanced colloidal stability. A series of HOOC–PHEA$_{73}$–PHBA$_{104-421}$ nano-objects prepared at pH 7 were characterized by visual inspection, DLS studies and shear-induced polarized light imaging. Discrepancies between these characterization techniques indicated that the worms and vesicles were unstable with respect to dilution. TEM studies were conducted after covalent stabilization of the nano-objects using glutaraldehyde (GA). More specifically, TEM studies of GA-crosslinked HOOC–PHEA$_{73}$–PHBA$_{243}$ and HOOC–PHEA$_{73}$–PHBA$_{421}$ nano-objects indicated the presence of spheres in both cases when crosslinked at 0.1% w/w and either worms or vesicles respectively when crosslinked at 10–20% w/w. Finally, HOOC–PHEA$_{73}$–PHBA$_{265}$ nano-objects were examined by variable temperature oscillatory rheology: thermoreversible sphere/worm and worm/vesicle transitions were observed between 2 and 50 °C.

Received 22nd November 2021,
Accepted 23rd December 2021

DOI: 10.1039/d1py01562a

rsc.li/polymers

Dainton Building, Department of Chemistry, University of Sheffield, Brook Hill, Sheffield, South Yorkshire, S3 7HF, UK. E-mail: s.p.armes@shef.ac.uk

†Electronic supplementary information (ESI) available: Experimental and characterization details; supporting figures, schemes and tables: assigned ^{1}H NMR spectra; summary table of DMF GPC and DLS data for a series of HOOC–PHEA$_{73}$–PHBA$_y$ dispersions; reaction scheme and DMF GPC curves for a one-pot synthesis of HOOC–PHEA$_{70}$–PHBA$_{100}$ at pH 2.5; acid titration curve for the HOOC–PHEA$_{73}$ precursor; normalized transmittance at 600 nm *vs.* temperature plot for a range of HOOC–PHEA$_x$ precursors; variation of apparent DLS diameter and zeta potential with pH; DLS particle size distributions at various salt concentrations; DMF GPC curves for a Mo–PHEA$_{76}$ precursor and a Mo–PHEA$_{76}$–PHBA$_{160}$ diblock copolymer; acid titration curve for the Mo–PHEA$_{76}$ precursor; SAXS patterns for HOOC–PHEA$_{70}$–PHBA$_{300}$ nano-objects; glutaraldehyde crosslinking scheme; summary table of TEM and variable temperature oscillatory rheology data for a range of HOOC-PHEA$_{73}$-PHBA$_y$ nano-objects. See DOI: 10.1039/d1py01562a

Introduction

Polymerization-induced self-assembly (PISA) offers a robust and highly versatile synthetic route to a wide range of well-defined block copolymer nano-objects in the form of concentrated colloidal dispersions.[1–8] PISA involves growing an insoluble block from one end of a soluble precursor block in a suitable solvent. Once some critical degree of polymerization is achieved for the insoluble block this causes micellar nucleation and ultimately leads to the formation of sterically-stabilized diblock copolymer nano-objects. The unreacted monomer acts as a processing aid (or co-solvent) and the high local monomer concentration within the monomer-swollen nanoparticles results in a relatively fast rate of polymerization com-

pared to the equivalent solution polymerization.[9,10] In the case of formulations based on dispersion polymerization, this approach is rather generic: PISA conducted in non-polar solvents, polar solvents or water seems to conform to essentially the same design rules.[11–14] PISA syntheses involving vinyl monomers are typically conducted using reversible addition–fragmentation chain transfer (RAFT) polymerization, which is well-known to be highly tolerant of monomer functionality.[8,15–19] In principle, the final copolymer morphology should depend on the relative volume fractions of the soluble and insoluble blocks.[20–22] In practice, various other synthesis parameters may also play important roles.[8,13,23–29] For aqueous PISA formulations, one important consideration seems to be the monomer solubility.[30–35] For example, there are various RAFT aqueous emulsion polymerization formulations involving sparingly-soluble vinyl monomers for which only kinetically-trapped spheres can be obtained.[36–39] In striking contrast, RAFT aqueous dispersion polymerization – for which the vinyl monomer must be water-miscible – usually provides access to the three most common copolymer morphologies (spheres, worms or vesicles) if the steric stabilizer block is not too long.[14,25,40,41]

It has become increasingly apparent that using such water-miscible monomers leads to the production of weakly hydrophobic structure-directing blocks that often exhibit thermoresponsive behavior.[42–45] Furthermore, morphological transitions can sometimes be induced simply by introducing a single charge at the end of the steric stabilizer block. This can be achieved either by ionization of a terminal carboxylic acid group[28,42,46] or by protonation of a terminal morpholine group.[47,48] Recently, we reported that diblock copolymer nano-objects prepared *via* RAFT aqueous dispersion polymerization can exhibit remarkable shape-shifting behavior.[42,49,50] More specifically, a *single* amphiphilic diblock copolymer can form spheres, worms, vesicles or lamellae in aqueous solution simply by varying the temperature from 1 °C to 70 °C.[42] In this case – which is particularly relevant to the present study – the steric stabilizer block was poly(*N,N*-dimethylacrylamide) (PDMAC) and diacetone acrylamide (DAAM) was statistically copolymerized with 4-hydroxybutyl acrylate (HBA) to produce a hydrophobic block that could be covalently crosslinked using adipic acid dihydrazide (ADH) to enable visualization of the copolymer morphologies using transmission electron microscopy (TEM).[42] Herein we replace the PDMAC stabilizer block with poly(2-hydroxyethyl acrylate) (PHEA), which has been previously used to produce a range of PHEA-stabilized nano-objects prepared by a post-polymerization solvent switch.[51–57] Recently, PHEA has been employed as a steric stabilizer for RAFT dispersion polymerization in either alcohol[58] or alcohol/water mixtures.[14,59,60] However, as far as we are aware PHEA has never been examined for purely aqueous PISA formulations. Moreover, we dispense with the DAAM comonomer and instead use glutaraldehyde to covalently stabilize hydroxyl-functional PHEA–PHBA diblock copolymer nano-objects for TEM studies. The sensitivity of such all-acrylic nanoparticles to changes in temperature, end-group ionization and serial dilution is explored and compared to prior PISA formulations.

One-pot synthesis of HOOC–PHEA–PHBA diblock copolymers *via* RAFT aqueous dispersion polymerization

According to the literature, the homopolymerization of HEA is typically conducted at high temperatures (*e.g.* 70 °C) in polar organic solvents such as DMF,[54–56,61] THF,[58] 1,4-dioxane,[14,59,60] various alcohols,[52,62,63] or mixtures thereof.[64,65] In contrast, there are far fewer reports of the RAFT solution polymerization of HEA in aqueous media, despite such reaction conditions being highly desirable for the development of efficient one-pot PISA syntheses of diblock copolymer nanoparticles. Thus, we decided to examine the RAFT aqueous solution polymerization of HEA at 44 °C using a trithiocarbonate-based carboxylic acid-functionalized RAFT agent (PETMP), see Scheme 1. We targeted 60% w/w solids so that the HEA monomer initially acted as a co-solvent to ensure RAFT agent solubility. A low-temperature thermal initiator was used to minimize chain transfer to polymer since this side reaction is well-known for acrylic polymerizations performed at elevated temperatures.[65,66] After 2.5 h, the crude HOOC–PHEA precursor was analyzed by DMF GPC and ^{1}H NMR spectroscopy. A relatively symmetrical GPC trace suggested minimal chain transfer to polymer during the polymerization, while the relatively narrow molecular weight distribution (M_w/M_n = 1.13, see Fig. 1A) indicates good RAFT control. ^{1}H NMR studies confirmed a final monomer conversion of 99%, which was calculated by comparing the integrated signal for the three vinyl protons assigned to the HEA monomer at 5.8–6.5 ppm to that of the five PETMP aromatic protons at 7.18–7.38 ppm (see Fig. S1B, ESI†). Moreover, a mean DP of 73 was determined for this HOOC–PHEA precursor after its isolation by precipitation (the integrated signals for the aromatic end-group at 7.18–7.38 ppm were compared to that of the oxymethylene proton signal at 4.18 ppm [Fig. S1B, ESI†]).

Subsequently, the crude HOOC–PHEA$_{73}$ precursor was chain-extended *via* RAFT aqueous dispersion polymerization of HBA at 44 °C, targeting 20% w/w solids and a range of PHBA DPs. For this second-stage polymerization, the solution pH was adjusted to pH 7 to ensure that the carboxylic acid group located on the end of each PHEA chain was present in its anionic carboxylate form. ^{1}H NMR studies indicated that more than 99% HBA conversion was achieved within 9 h for all target copolymer compositions, as determined by comparing the integrated HBA vinyl signals at 5.8–6.5 ppm to the integrated PHBA signal at 3.63 ppm (Fig. S1C, ESI†). Similarly, final diblock copolymer compositions (Table S1, ESI†) were determined by comparing the PHEA signal at 3.78 ppm with the PHBA signal at 3.63 ppm (Fig. S1C, ESI†). DMF GPC studies indicated reasonably high blocking efficiencies (see Fig. 1A) and a relatively linear evolution of M_n with PHBA DP (see Fig. 1B).

Notably each of the diblock copolymer GPC traces shown in Fig. 1A contains a high molecular weight shoulder, which becomes more prominent when targeting higher PHBA DPs.

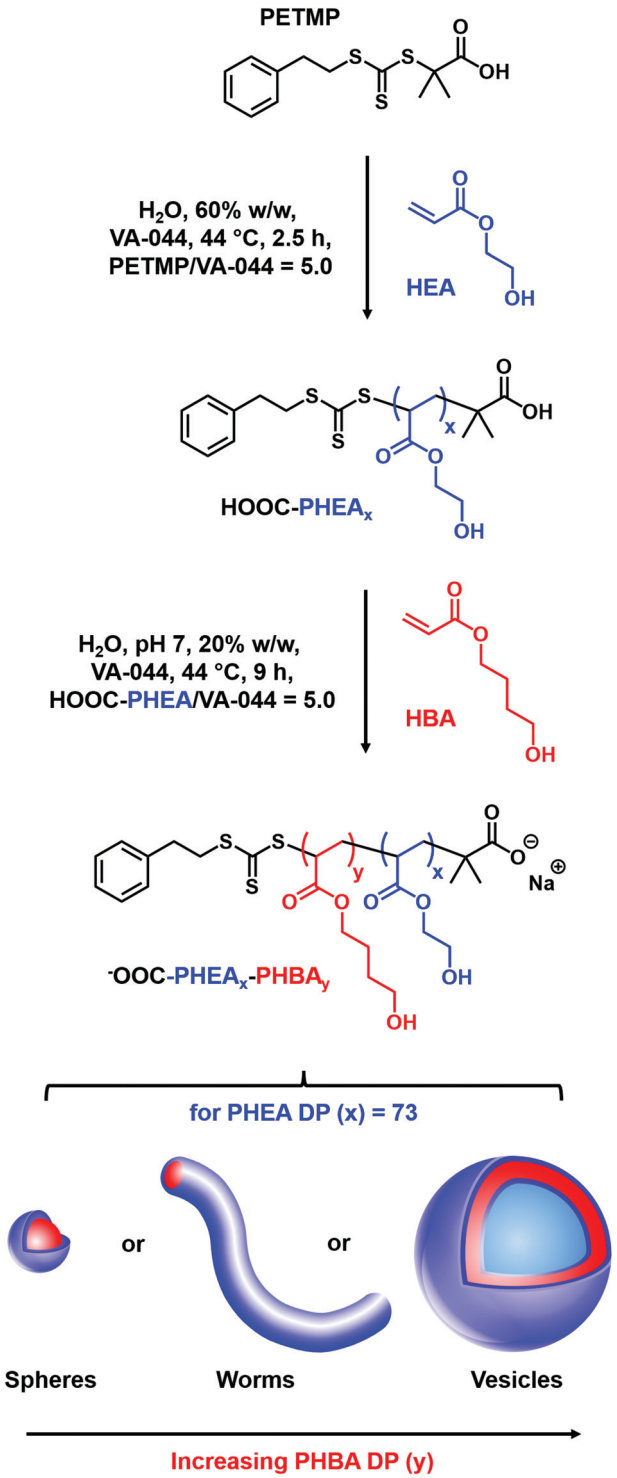

Scheme 1 Reaction scheme outlining the one-pot synthesis of HOOC–$PHEA_x$–$PHBA_y$ diblock copolymer nano-objects at pH 7 *via* RAFT aqueous dispersion polymerization of HBA. First, a HOOC–$PHEA_x$ precursor is prepared at 60% w/w solids *via* RAFT aqueous solution polymerization of HEA at 44 °C using a carboxylic acid-based RAFT agent (PETMP). The crude HOOC–$PHEA_x$ precursor is then used for the RAFT aqueous dispersion polymerization of HBA at pH 7 without further purification. In principle, aqueous dispersions of spheres, worms or vesicles should be accessible depending on the precise PHBA DP provided that the HOOC–$PHEA_x$ precursor is not too long (*e.g.*, x = 73).

There is a corresponding broadening of the molecular weight distribution (see Fig. 1B and Table S1, ESI†), with dispersities increasing gradually up to a PHBA DP of 316, before rising more rapidly for higher DPs. This is most likely the result of chain transfer to polymer[65,66] and/or light branching owing to trace amounts of diacrylate impurities in the HBA monomer.[67,68] It is perhaps worth emphasizing that appropriate steps were taken to minimize such problems: the HBA monomer was extensively purified *via* exhaustive solvent extraction with *n*-hexane to remove diacrylate impurities and its subsequent polymerization was conducted at a relatively low temperature (44 °C).

In developing this PISA protocol, it became apparent that the resulting HOOC–$PHEA_{73}$–$PHBA_y$ diblock copolymer nano-objects exhibited unusual colloidal stability behavior. In initial experiments, a one-pot synthesis protocol similar to that reported by Byard *et al.*[42] for the preparation of PDMAC-P (HBA-*stat*-DAAM) diblock copolymer nano-objects was explored (see Fig. S2A, ESI†). This involved synthesis of a new HOOC–$PHEA_{70}$ precursor at 60% w/w solids using a redox initiator at 30 °C. Within 1.75 h, >99% HEA conversion was achieved and the subsequent RAFT aqueous dispersion polymerization of HBA was conducted at pH 2.5 targeting 20% w/w solids. However, macroscopic phase separation unexpectedly occurred forming two distinct layers (see Fig. S2B, ESI†). DMF GPC studies conducted on the precursor, the viscous yellow lower layer and the free-flowing transparent upper layer confirmed that chain extension had occurred but the upper layer contained some unreacted HOOC–$PHEA_{70}$ precursor (see Fig. S2B, ESI†). One important difference between this initial synthesis route and that shown in Scheme 1 is the solution pH. The carboxylic acid end-group located on each PHEA steric stabilizer chain is ionized at pH 7.0, whereas it is in its neutral form at pH 2.5. According to our prior studies, this subtle difference can significantly affect the aqueous solubility of a weakly hydrophilic water-soluble polymer.[69] Accordingly, we undertook a series of experiments as a function of solution pH to examine the reason for the unexpected poor colloidal stability observed at pH 2.5.

Effect of varying the solution pH on colloidal stability

Dynamic light scattering (DLS) and aqueous electrophoresis studies were conducted by adjusting the pH of a 0.1% w/w aqueous dispersion of HOOC–$PHEA_{73}$–$PHBA_{217}$ nanoparticles prepared according to Scheme 1 (Fig. 2A). Between pH 10 and pH 5.5, the *z*-average diameter remained constant at approximately 35 nm. Within this pH range, the zeta potential only varied between −16 and −20 mV, with the slightly less negative zeta potentials observed between pH 6.5 and 5.5 coinciding with a modest increase in the particle size. However, lowering the pH to 5.1 led to significant flocculation: the apparent *z*-average diameter more than doubled to 108 nm, although the zeta potential was only marginally lower at −14.6 mV. Interestingly, this onset of aggregation coincides with the pK_a determined for the HOOC–$PHEA_{73}$ precursor (see Fig. S3, ESI†). This suggests that the HOOC–$PHEA_{73}$–$PHBA_{217}$ nano-

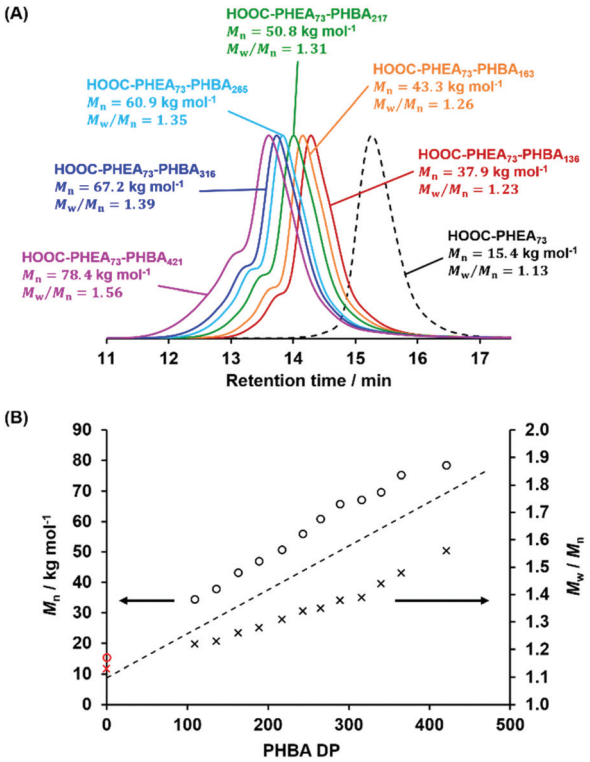

Fig. 1 (A) DMF GPC curves (refractive index detector; expressed relative to a series of poly[methyl methacrylate] [PMMA] calibration standards) recorded for the HOOC–$PHEA_{73}$ precursor (dotted curve) and selected HOOC–$PHEA_{73}$–$PHBA_y$ diblock copolymers (solid curves) prepared at pH 7. (B) The corresponding evolution in number-average molecular weight (M_n, open circles) and dispersity (M_w/M_n, crosses) with PHBA DP (raw data provided in Table S1, ESI†). Data for the HOOC–$PHEA_{73}$ precursor are indicated by the red data points marked on the *y* axis (PHBA DP = 0) and account for the non-zero intercepts while the dashed line indicates the theoretical M_n.

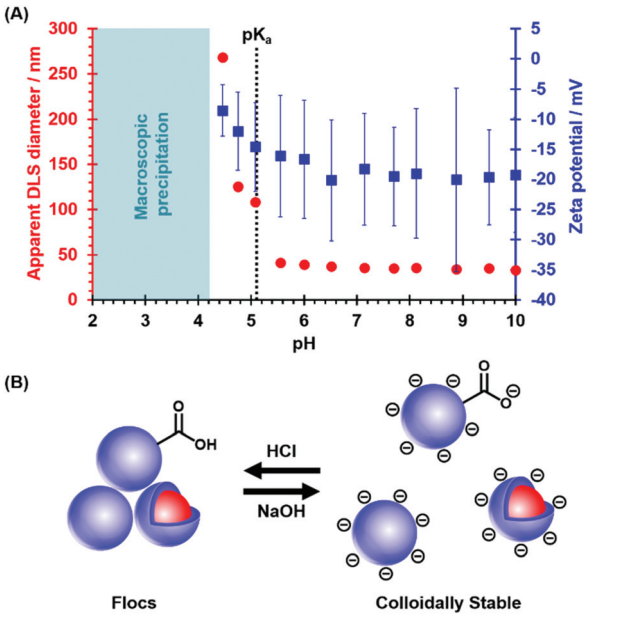

Fig. 2 (A) Variation in apparent *z*-average diameter (red circles) and zeta potential (blue squares) with solution pH for a 0.1% w/w aqueous dispersion of HOOC–$PHEA_{73}$–$PHBA_{217}$ nanoparticles at 25 °C in the presence of 1 mM KCl. The vertical black dotted line indicates the pK_a of 5.1 as determined by acid titration of the HOOC–$PHEA_{73}$ precursor (see Fig. S3, ESI†). (B) Schematic representation of the protonation of carboxylic acid end-groups on the PHEA steric stabilizer chains that causes nanoparticle flocculation below pH 5.5.

particles require more than 50% of their carboxylic acid end-groups to be ionized to retain colloidal stability, as schematically illustrated in Fig. 2B. Lowering the pH further results in a correspondingly higher degree of flocculation. Macroscopic precipitation was observed at around pH 4.5, for which the zeta potential was approximately −8.5 mV. These data are consistent with the formation of colloidally unstable nano-objects when performing the RAFT aqueous dispersion polymerization of HBA when using a HOOC–$PHEA_{70}$ precursor at pH 2.5.

In related work, Gibson *et al.*[69] found that colloidal dispersions of poly(*N*-2-(methacryloyloxy)ethyl pyrrolidone)-poly(2-hydroxypropyl methacrylate) (PNMEP–PHPMA) nanoparticles could be prepared using a similar carboxylic acid-functionalized RAFT agent at pH 7, but not at pH 3. In this prior study, ionization of such end-groups is critical for colloidal stability since this raises the cloud point for the HOOC–$PNMEP_x$ stabilizer block by up to 25 °C. For PISA syntheses conducted at 44 °C, this represents the difference between effective steric stabilization and colloidal instability.[69]

However, PHEA should not exhibit such inverse temperature solubility: according to the literature, it should exhibit a cloud point above 100 °C.[70] Indeed, turbidimetry studies conducted between 25 and 90 °C on 1.0% w/w dispersions of three HOOC–$PHEA_x$ precursors (x = 49, 72 or 100) indicated no significant change in transmittance at either pH 2.5 or pH 7.0. Clearly, regardless of whether their carboxylic acid end-groups are ionized or not, these three HOOC–$PHEA_x$ precursors possess cloud points above 90 °C (see Fig. S4, ESI†). Thus, although ionization of carboxylic acid end-groups is certainly essential for the successful aqueous PISA synthesis of HOOC–$PHEA_{73}$–$PHBA_y$ nano-objects, this appears to involve a subtly different mechanism to that reported by Gibson *et al.*[69] for HOOC–$PNMEP_x$–$PHPMA_y$ nano-objects.

The acid-induced flocculation of the HOOC–$PHEA_{73}$–$PHBA_{217}$ nanoparticles shown in Fig. 2 was found to be reasonably reversible: after a pH 10 – pH 2 – pH 10 cycle, DLS studies indicated that, above pH 6.5, the apparent nanoparticle diameter was only slightly larger than the initial value (see Fig. S5, ESI†). This modest increase in size is likely to be the result of the build-up of background salt, which would also account for the slightly less negative zeta potentials. Such nanoparticle redispersion is in good agreement with the reversible pH-responsive behavior reported for similar sterically-stabilized diblock copolymer nanoparticles by Lovett and co-workers,[28] Penfold *et al.*[47] and Byard *et al.*[42] However, it is in contrast to the *irreversible* aggregation behavior reported by Gibson and co-workers.[69]

Next, the effect of added salt on colloid stability was examined. Thus, a series of 0.1% w/w aqueous dispersions of

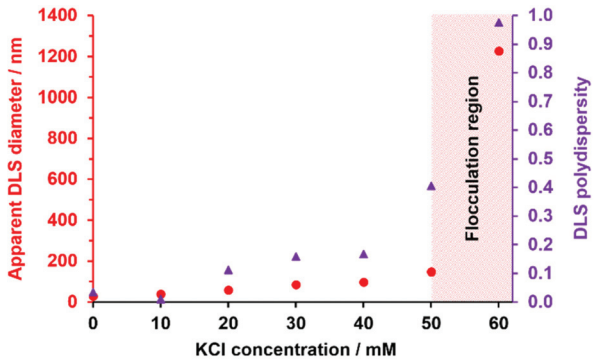

Fig. 3 Variation in apparent *z*-average diameter (red circles) and polydispersity (purple triangles) with KCl concentration indicated by DLS studies of a 0.1% w/w aqueous dispersion of HOOC–$PHEA_{73}$–$PHBA_{217}$ nanoparticles at pH 7 (see also Fig. S6, ESI†).

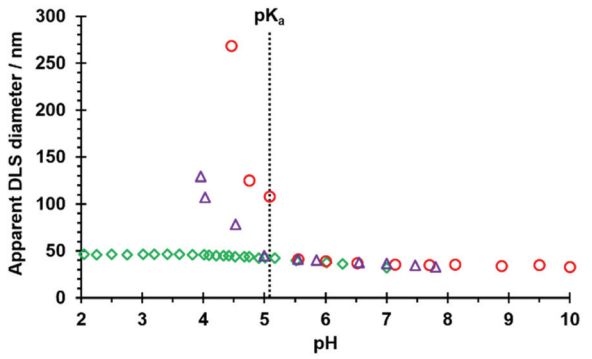

Fig. 4 Variation in apparent *z*-average diameter with pH observed for 0.1% w/w aqueous dispersions of HOOC–$PHEA_{73}$–$PHBA_{217}$ (red circles), HOOC–$PHEA_{105}$–$PHBA_{194}$ (purple triangles) and HOOC–$PHEA_{140}$–$PHBA_{205}$ (green diamonds) nanoparticles at 25 °C in the presence of 1 mM KCl. Measurements were performed by titrating from high pH using aqueous HCl. The vertical black dotted line indicates the pK_a of 5.1 determined for each of the HOOC–$PHEA_x$ precursors by acid titration.

HOOC–$PHEA_{73}$–$PHBA_{217}$ nanoparticles were prepared in the presence of KCl and their apparent *z*-average particle diameters were assessed by DLS at pH 7 (see Fig. 3). As expected, the colloidal stability was very sensitive to the salt concentration, with the apparent particle size doubling in the presence of only 20 mM KCl (see Fig. 3 and Fig. S6A, ESI†). Moreover, multimodal particle size distributions were obtained as the salt concentration was raised to 50–60 mM KCl, indicating extensive flocculation under such conditions (see Fig. S6B, ESI†). This suggests that the nanoparticle aggregation observed in the presence of added salt is the result of charge screening of the anionic carboxylate end-groups. As noted above, the HOOC–$PHEA_{73}$ block is not sufficiently long to confer efficient steric stabilization in its neutral form. Given that the HOOC–$PHEA_{73}$–$PHBA_{217}$ nanoparticles exhibit both pH- and salt-dependent colloidal stability, this is consistent with an electrosteric stabilization mechanism.[69,71,72]

Once the pH-dependent colloidal stability of HOOC–$PHEA_{73}$–$PHBA_{217}$ nanoparticles was established, the effect of adjusting the HOOC–PHEA stabilizer DP while maintaining a similar PHBA DP (*i.e.* varying the HBA/HEA molar ratio) was investigated. More specifically, HOOC–$PHEA_{105}$–$PHBA_{194}$ and HOOC–$PHEA_{140}$–$PHBA_{205}$ dispersions (HBA/HEA molar ratios = 1.8 and 1.5, respectively) were prepared at pH 7 and then DLS and aqueous electrophoresis studies were conducted as a function of pH (see Fig. 4). Fig. 4 indicates that the critical pH for flocculation can be suppressed by increasing the DP of the stabilizer block, with aggregation being observed at pH 5.1 and pH 4.5 for the HOOC–$PHEA_{73}$–$PHBA_{217}$ and HOOC-$PHEA_{105}$–$PHBA_{194}$ nanoparticles, respectively. Thus, increasing the DP of the HOOC–$PHEA_x$ block reduces the fraction of stabilizer chains bearing anionic carboxylate end-groups required to maintain colloidal stability. Moreover, the HOOC–$PHEA_{140}$–$PHBA_{205}$ dispersion remains colloidally stable across the entire pH range. This suggests that there is a critical DP above which (and/or a critical HBA/HEA molar ratio below which) end-group ionization is no longer required to confer colloidal stability to such nanoparticles, *i.e.* purely steric stabilization is sufficient to prevent aggregation.

To investigate whether the enhanced colloidal stability observed for the HOOC–$PHEA_{140}$–$PHBA_{205}$ dispersion in Fig. 4 is the result of a longer PHEA DP or a lower HBA/HEA molar ratio, the colloidal stability of a HOOC–$PHEA_{140}$–$PHBA_{408}$ dispersion was studied over the same pH range. This diblock copolymer has a PHBA/PHEA molar ratio of 2.9, which is very similar to that for the HOOC–$PHEA_{73}$–$PHBA_{217}$ diblock copolymer (PHBA/PHEA molar ratio = 3.0), thus enabling a meaningful comparison of the pH-dependence of their colloidal stability. Accordingly, DLS and aqueous electrophoresis studies were performed on a 0.1% w/w aqueous dispersion of HOOC–$PHEA_{140}$–$PHBA_{408}$ nanoparticles. In Fig. 5A and B, these data are compared with that obtained for the HOOC–$PHEA_{73}$–$PHBA_{217}$ nanoparticles shown in Fig. 2. Similar behavior is observed above pH 5.1, which corresponds to the common pK_a value obtained for the two corresponding stabilizer chains: the particle size remains around 50 nm on lowering the pH from 7.7 to 5.5 (see Fig. 5A) and there is a concomitant modest reduction in zeta potential (see Fig. 5B). However, the two types of nanoparticles exhibit divergent behavior below pH 5.1. As previously noted, the apparent *z*-average diameter of the HOOC–$PHEA_{73}$–$PHBA_{217}$ nanoparticles increases dramatically, indicating the onset of flocculation. In contrast, the apparent *z*-average diameter for the HOOC–$PHEA_{140}$–$PHBA_{408}$ nanoparticles gradually increases on lowering the pH from 5.0 to 4.3 before attaining a constant value of approximately 103 nm below pH 4.3 (see Fig. 5A). Meanwhile, the corresponding zeta potential is reduced from −8.2 mV at pH 5.0 to approximately −0.5 mV at pH 2.0 (see Fig. 5B). This indicates that these nanoparticles retain a reasonably high degree of dispersion in the form of relatively small flocs at low pH, despite the absence of any anionic end-groups under such conditions. Furthermore, these data suggest that longer HOOC–PHEA stabilizer chains confer more effective steric stabilization and do not require end-group ionization to prevent macroscopic precipitation.

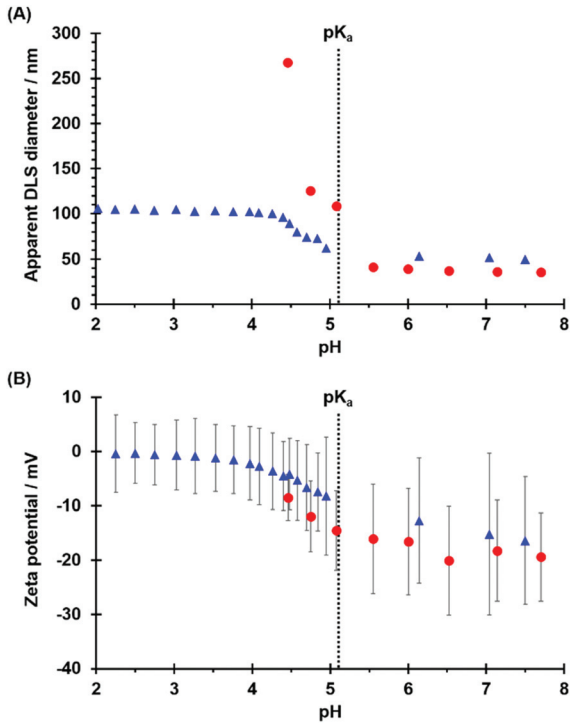

Fig. 5 Variation in (A) the apparent *z*-average diameter and (B) zeta potential with pH observed for 0.1% w/w aqueous dispersions of HOOC–PHEA$_{73}$–PHBA$_{217}$ nanoparticles (red circles) and HOOC–PHEA$_{140}$–PHBA$_{408}$ nanoparticles (blue triangles) at 25 °C in the presence of 1 mM KCl. Measurements were performed by titrating from high pH using aqueous HCl. The vertical black dotted lines indicate the pK_a of 5.1 determined for each of the HOOC–PHEA$_x$ precursors by acid titration.

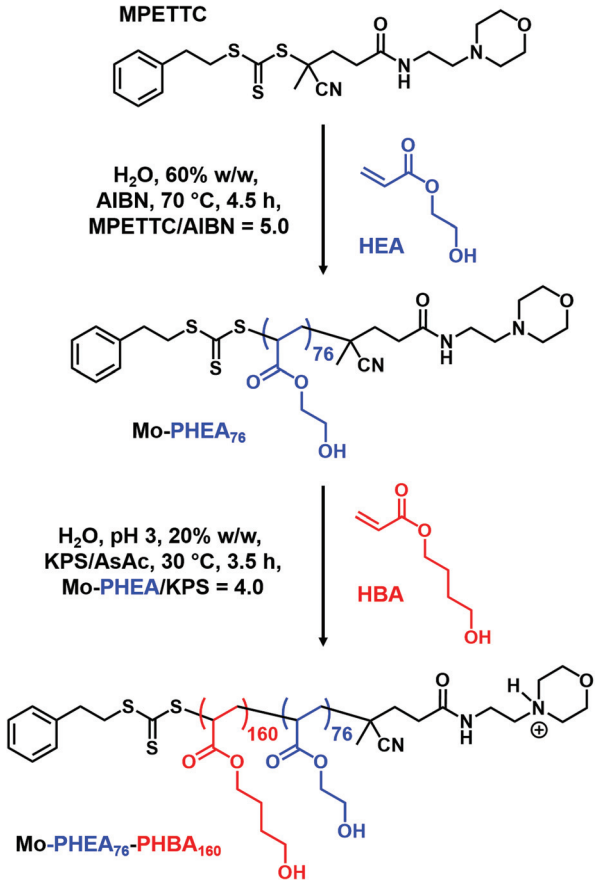

Scheme 2 Reaction scheme for the one-pot PISA synthesis of Mo–PHEA$_{76}$–PHBA$_{160}$ nanoparticles at pH 3. First, the Mo–PHEA$_{76}$ precursor is prepared *via* RAFT aqueous solution polymerization of HEA at 70 °C targeting 60% w/w solids using a morpholine-based RAFT agent (MPETTC). This Mo–PHEA$_{76}$ precursor is then used directly without further purification to conduct the RAFT aqueous dispersion polymerization of HBA at 30 °C using a potassium persulfate/ascorbic acid (KPS/AsAc) redox initiator at pH 3.

Tailoring colloidal stability *via* choice of RAFT agent

Bearing in mind the above end-group effect, we decided to evaluate a morpholine-functionalized RAFT agent (MPETTC) for the aqueous PISA synthesis of Mo–PHEA$_x$–PHBA$_y$ nanoparticles, where Mo denotes an 2-(*N*-morpholino)ethyl end-group. In principle, such dispersions should exhibit *complementary* pH-dependent colloidal stability. Accordingly, Mo–PHEA$_{76}$–PHBA$_{160}$ nanoparticles were prepared using MPETTC at pH 3 targeting 20% w/w solids according to the one-pot protocol outlined in Scheme 2. Analysis of the Mo–PHEA$_{76}$ precursor and final diblock copolymer by ^{1}H NMR spectroscopy confirmed that 99% conversion was achieved for each step, while DMF GPC analysis indicated relatively narrow molecular weight distributions in each case (M_w/M_n = 1.15 and 1.35, respectively) and a reasonably high blocking efficiency (see Fig. S7A, ESI†). Importantly, the resulting aqueous dispersion showed no signs of flocculation at pH 3 (see Fig. S7A, ESI†), suggesting good colloidal stability under such conditions.

DLS and electrophoresis studies were conducted on a 0.1% w/w aqueous dispersion of the Mo–PHEA$_{76}$–PHBA$_{160}$ nanoparticles (see Fig. 6A). As expected, the apparent *z*-average diameter remained constant at approximately 42 nm below pH 5, while zeta potentials ranged from +5.9 to +8.5 mV. However, weak flocculation was evident at pH 5.6, for which the zeta potential was +3.3 mV. Above pH 5.7, the apparent DLS size exceeded the 6 μm upper limit for the DLS instrument, indicating macroscopic precipitation (see Fig. 6B). Thus, complete loss of colloidal stability occurs well below the pK_a of 6.4 determined for the conjugate acid form of the morpholine end-groups on the PHEA stabilizer chains (see Fig. S7B, ESI;† this pK_a is in good agreement with that reported by Penfold *et al.* for a PGMA$_{50}$ homopolymer prepared using MPETTC).[47] This suggests that a relatively high proportion of morpholine end-groups must be protonated to maintain colloidal stability.

Effect of dilution on the morphology of HOOC–PHEA$_{73}$–PHBA$_y$ nano-objects

Fig. 7 indicates the visual appearance at 25 °C of a series of 20% w/w aqueous dispersions of HOOC–PHEA$_{73}$–PHBA$_y$ nanoparticles prepared at pH 7. These dispersions remain transparent up to a PHBA DP of 265, above which they become increasingly turbid. The four central inverted vials indicate that the dispersion viscosity increases monotonically up to a maximum

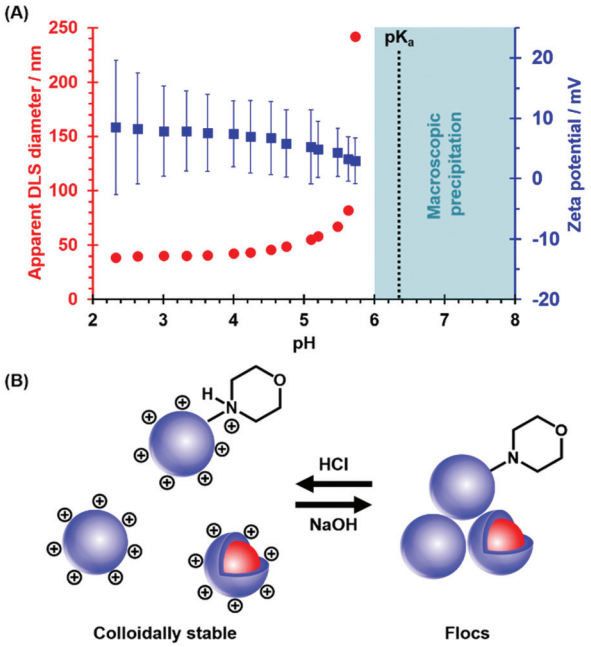

Fig. 6 (A) Variation in apparent z-average diameter (red circles) and zeta potential (blue squares) with solution pH observed for a 0.1% w/w aqueous dispersion of Mo–PHEA$_{76}$–PHBA$_{160}$ nanoparticles at 25 °C in the presence of 1 mM KCl. The vertical black dotted line indicates the pK_a of 6.4 determined for the Mo–PHEA$_{76}$ precursor by acid titration. (B) Schematic representation of the (de)protonation of the morpholine end-group that results in nanoparticle flocculation at higher pH, as indicated by the DLS data shown in (A).

value at a PHBA DP of 265, with free-flowing milky-white dispersions being obtained at higher PHBA DPs. Based on our previous experience of various PISA formulations,[42,73,74] this strongly suggests the formation of transparent dispersions of free-flowing spheres (y = 109–189), relatively transparent worm gels (y = 217–289), and relatively turbid vesicles (y = 316–421).

Accordingly, DLS studies were conducted on 0.1% w/w aqueous dispersions of HOOC–PHEA$_{73}$–PHBA$_y$ nanoparticles at pH 7 after sequential dilution (see Fig. 8 and Table S1, ESI†). As shown in Fig. 8A, the apparent z-average diameter at 25 °C increased linearly from 14 nm to 52 nm with PHBA DP. Moreover, particle size distributions were relatively narrow, with most dispersions exhibiting DLS polydispersities below 0.10. These observations are precisely what would be expected for a series of kinetically-trapped spheres.[75–77] However, this is clearly not consistent with the visual appearance of the series of 20% w/w aqueous dispersions shown in Fig. 7. For example, nanoparticles with an apparent z-average diameter of 33 nm should not form a transient free-standing gel, as observed for the 20% w/w HOOC–PHEA$_{73}$–PHBA$_{265}$ dispersion. Similarly, aqueous dispersions with z-average diameters ranging from 35 to 52 nm should not exhibit strong turbidity (as shown in Fig. 7 for 20% w/w HOOC–PHEA$_{73}$–PHBA$_y$ nanoparticles when $y \geq 289$). Furthermore, the DLS data do not suggest that such turbidity results from colloidal instability. Instead, these observations suggest that (some of) the nano-objects are unstable with respect to dilution, with worms or vesicles undergoing *in situ* dissociation to form relatively large spheres. As far as we are aware, such dilution instability is seldom reported for PISA-synthesized nano-objects.[45] Nevertheless, this explanation is consistent with the relatively narrow DLS particle size distributions, small z-average diameters and the linear increase in apparent nanoparticle diameter with PHBA DP.[75] Moreover, we have recently reported that the structure-directing PHBA block is only weakly hydrophobic.[42,50]

Even without the additional complication of dilution-induced instability, assigning morphologies for acrylic diblock copolymer nano-objects is generally rather more problematic than for the corresponding methacrylic nano-objects.[14,42,51,73,78,79] This is because the former nano-objects typically exhibit a sub-ambient glass transition temperature (T_g), which prevents conventional TEM analysis owing to nanoparticle deformation and/or film formation during grid preparation. In principle, cryo-TEM can be used to image such low T_g nanoparticles.[29,73] However, *in situ* dilution is required for cryo-TEM sample preparation. Alternatively, small-angle X-ray scattering (SAXS) can readily distinguish between spheres, worms and vesicles and this technique can be conducted at relatively high copolymer concentration.[80–82] However, a structure factor is typically observed under such conditions; this

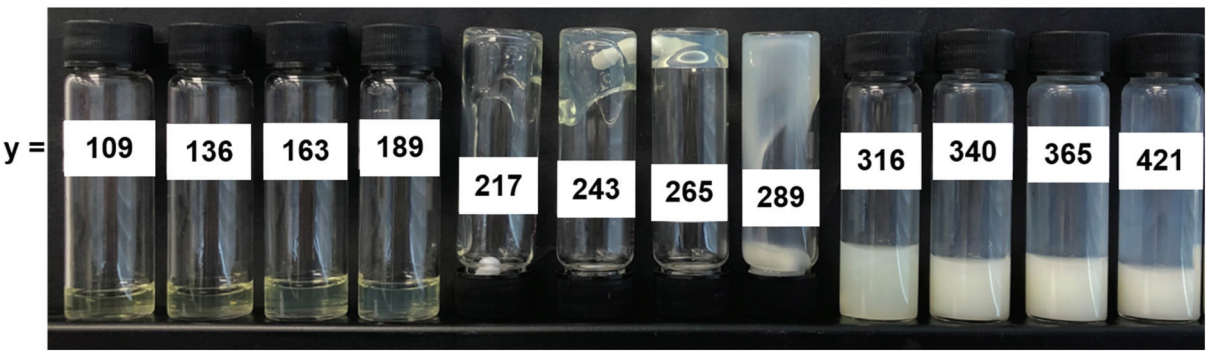

Fig. 7 Digital photograph recorded at 25 °C indicating the physical appearance of a series of as-synthesized 20% w/w aqueous dispersions of HOOC–PHEA$_{73}$–PHBA$_y$ nano-objects (where y varies from 109 to 421, see tube labels) prepared at pH 7 according to the protocol outlined in Scheme 1.

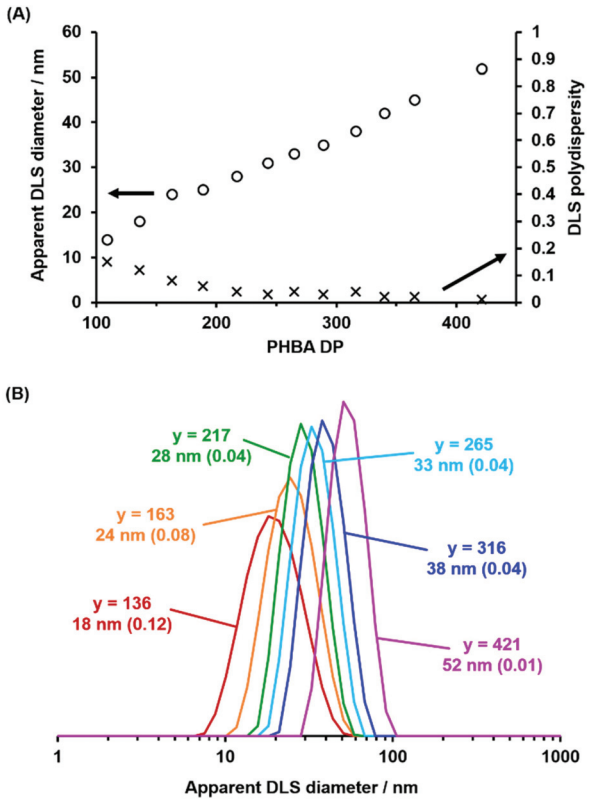

Fig. 8 (A) Variation of the apparent DLS diameter, D_h (circles) and DLS polydispersity (PDI, crosses) with PHBA DP (y) for a series of 0.1% w/w aqueous dispersions of HOOC–PHEA$_{73}$–PHBA$_y$ nano-objects at pH 7. (B) DLS size distributions recorded for selected nano-objects (see also Table S1, ESI†).

significantly complicates the data analysis, particularly for worms (see Fig. S8, ESI†). Indeed, SAXS patterns recorded at 1.0% w/w for the charged nano-objects described herein exhibit a pronounced structure factor arising from strong inter-particle electrostatic repulsion (see Fig. S8B, ESI†). Such interactions also have consequences for DLS measurements, whereby the incurred systematic error leads to an apparent particle diameter (see Fig. 2A, 3, 4, 5A, 6A and 8A).

An alternative approach is nanoparticle crosslinking: we have recently reported that such covalent stabilization can facilitate nano-object imaging by conventional TEM.[42,50] For example, Deane *et al.* utilized the pendent hydroxyl group present in each PHBA residue as a reactive site for crosslinking using a well-known biological fixative, glutaraldehyde (GA).[50,83] Importantly, such covalent stabilization should allow TEM studies of the original HOOC–PHEA$_{73}$–PHBA$_y$ spheres, worms and vesicles and also any new nano-objects that may be formed on dilution.

Accordingly, a transparent, free-flowing dispersion of HOOC–PHEA$_{73}$–PHBA$_{136}$ nano-objects (tentatively assigned as spheres) and a turbid, free-flowing dispersion of HOOC–PHEA$_{73}$–PHBA$_{421}$ nano-objects (tentatively assigned as vesicles) were each crosslinked in turn at 20 °C at either 0.1 or 10% w/w (see Scheme S1, ESI†). Similarly, HOOC–PHEA$_{73}$–PHBA$_{243}$ nano-objects (tentatively assigned as worms) were crosslinked in the form of a 20% w/w transparent gel at 40 °C, which corresponds to the critical gelation temperature (CGT, see Fig. S9B and Scheme S1, ESI†) and also under the same conditions after dilution to 0.1% w/w. TEM studies (see Fig. 9) revealed the presence of small HOOC–PHEA$_{73}$–PHBA$_{136}$ spheres at 20 °C regardless of whether GA crosslinking is conducted at 10 or 0.1% w/w. Furthermore, there was no evidence for interparticle crosslinking when conducting such experiments at 10% w/w, despite the presence of reactive hydroxyl groups within the PHEA stabilizer chains (see Table S2, ESI†). Conversely, GA crosslinking the HOOC–PHEA$_{73}$–PHBA$_{243}$ nano-objects at 20% w/w reveals the presence of anisotropic worm-like nanoparticles, whereas only isotropic spherical nanoparticles are obtained after covalent stabilization at 0.1% w/w. Similarly, TEM studies of PHEA$_{73}$–PHBA$_{421}$ nano-objects crosslinked at 10% w/w indicate the presence of large vesicles, as expected given the turbid appearance of such dispersions. In contrast, GA crosslinking at 0.1% w/w afforded much smaller spheres. These observations are consistent with the corresponding DLS data obtained for the linear nano-objects at 0.1% w/w. In summary, these DLS and TEM studies provide strong evidence for the instability of HOOC–PHEA$_{73}$–PHBA$_y$ worms and vesicles with respect to spheres on serial dilution.

Characterization of concentrated dispersions

In order to further examine the morphology of the as-synthesized aqueous dispersions of HOOC–PHEA$_{73}$–PHBA$_y$ nanoparticles, alternative analytical techniques applicable to concentrated dispersions were required. Thus, the series of 20% w/w HOOC–PHEA$_{73}$–PHBA$_y$ nanoparticles was studied using shear-induced polarized light imaging (SIPLI) at 25 °C. SIPLI is an opto-rheological technique that enables the presence of

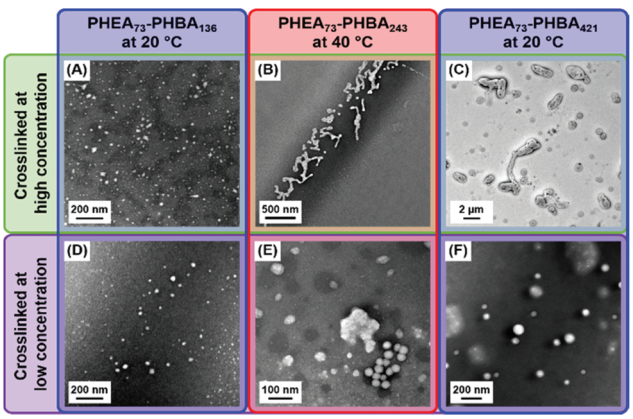

Fig. 9 TEM images recorded for dilute aqueous dispersions of HOOC–PHEA$_{73}$–PHBA$_{136}$ nano-objects crosslinked at 20 °C (A and D); HOOC–PHEA$_{73}$–PHBA$_{243}$ nano-objects crosslinked at 40 °C (B and E), and HOOC–PHEA$_{73}$–PHBA$_{421}$ nano-objects crosslinked at 20 °C (C and F). In each case GA crosslinking was conducted at pH 7 using a GA/HBA molar ratio of 0.66 at either 10–20% w/w concentration (A–C) or 0.1% w/w concentration (D–F).

anisotropic nanoparticles to be identified *via* the appearance of a characteristic Maltese cross motif.[45,84,85] This feature is the result of the birefringence generated by *in situ* alignment of the anisotropic particles under shear. Furthermore, the plate-plate geometry utilized for SIPLI experiments results in a continuous gradient of shear rates radially distributed from zero to a maximum value at the disk edge. This allows the critical shear rate required for the alignment of anisotropic particles to be identified, where the central dark area of the Maltese cross transitions to the light area, indicating alignment. If no Maltese cross is observed, this indicates the presence of isotropic nanoparticles. Therefore, this technique should enable highly anisotropic worms to be identified if such species are present in the as-synthesized concentrated aqueous dispersions of HOOC–$PHEA_{73}$–$PHBA_y$ nanoparticles.

Angular speed sweeps were conducted between 0.0008 and 8 rad s^{-1} (corresponding to maximum shear rates at the disk edge of 0.01 and 100 s^{-1}) with polarized light images being captured periodically as the maximum shear rate was gradually increased. A representative polarized light image recorded at 25 °C for each dispersion of HOOC–$PHEA_{73}$–$PHBA_y$ nanoparticles is shown in Fig. 10. These images were recorded at various shear rates depending on whether a Maltese cross was observed or not; if this feature appeared, then the shear rate was adjusted to achieve the optimal image in each case. Morphologies were assigned based on these SIPLI images taking into account the visual appearance of each 20% w/w aqueous copolymer dispersion at 25 °C, see Fig. 7.

For 20% w/w HOOC–$PHEA_{73}$–$PHBA_y$ dispersions with y = 109 or 136, no Maltese cross was observed up to a maximum shear rate of 100 s^{-1} (see Fig. 10). This is consistent with the presence of isotropic spherical nanoparticles, with mean apparent diameters indicated by DLS studies of the corresponding diluted dispersions (Fig. 8). As y is increased from 163 to 217, a Maltese cross is observed at a progressively lower maximum shear rate (ranging from 100 s^{-1} to 8 s^{-1}), with this feature gradually becoming more intense. Since the dispersion viscosity clearly increases with PHBA DP (see Fig. 7), this suggests the presence of a mixed phase comprising isotropic spheres and (increasingly) anisotropic worms for such copolymer compositions. This is commonly observed for PISA formulations that lie intermediate between pure spheres and pure worms.[25,58,86] As y is increased further to 243 or 265, intense Maltese crosses are obtained at lower maximum shear rates (2 and 0.8 s^{-1} respectively, see Fig. 10); this is not unexpected given that such dispersions form transparent viscous fluids (Fig. 7), which suggests the presence of highly anisotropic linear worms. The dispersions become more turbid and less viscous for y = 289–421. Nevertheless, Maltese crosses were still observed over this range at relatively low maximum shear

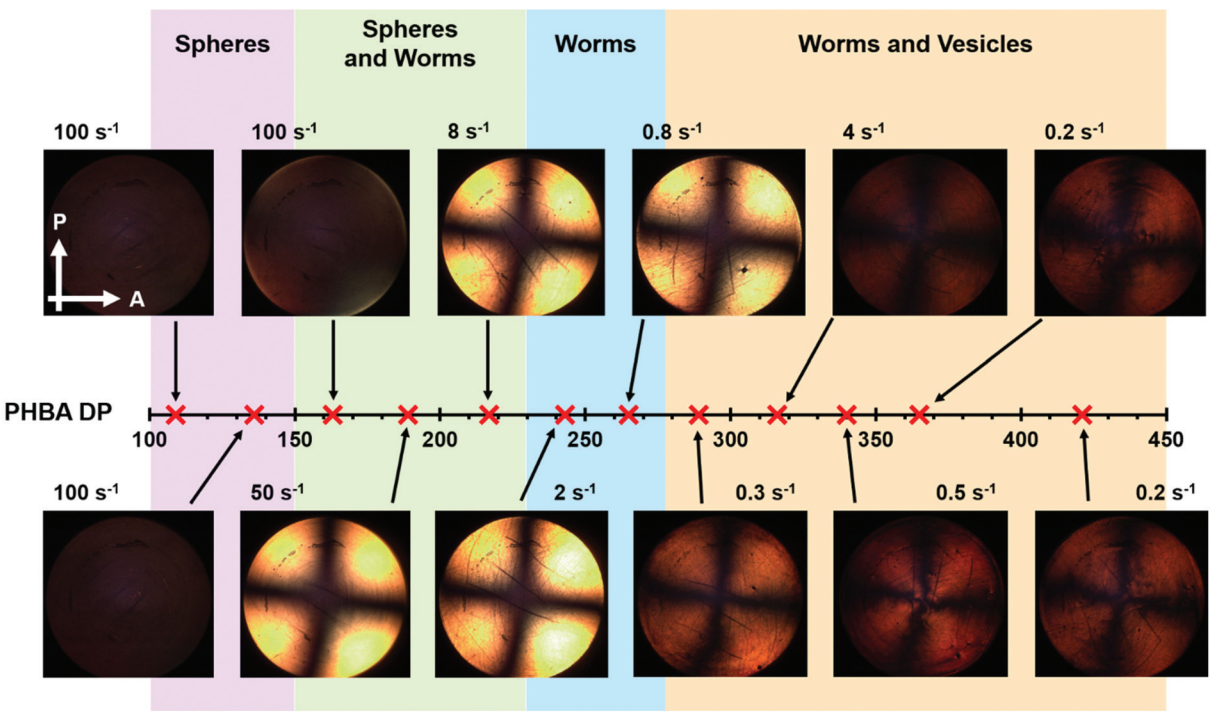

Fig. 10 Digital polarized light images recorded under shear at various maximum shear rates (0.2–100 s^{-1}) when conducting SIPLI experiments at 25 °C on a series of 20% w/w aqueous dispersions of HOOC–$PHEA_{73}$–$PHBA_y$ nano-objects (y = 109–421; see red crosses marked on the horizontal PHBA DP axis). The optimized maximum (sample edge) shear rate at which each dispersion was assessed is stated for each polarized light image. Shaded regions indicate the assigned morphology based on the presence or absence of a Maltese cross, the corresponding shear rate and the visual appearance of each copolymer dispersion at 25 °C (see Fig. 8). The white arrows indicate the relative orientation of the polarizer (P) with respect to the analyzer (A) planes, respectively.

rates between 4 and 0.2 s^{-1}. This suggests that a mixed phase comprising worms and vesicles persists over this compositional range, with a gradual increase in the proportion of the latter species accounting for the increase in turbidity (see Fig. 7).

It is perhaps surprising that a worm population appears to persist over such a wide range of copolymer compositions.[25] However, it is likely that the anionic surface charge required to ensure electrosteric stabilization of these nano-objects impedes the worm-to-vesicle transition as the PHBA DP is increased, thereby delaying the formation of pure vesicles. Indeed, it is well documented in the PISA literature that introducing charge into the steric stabilizer chains often prevents (or delays) the formation of worms or vesicles.[27,87] Furthermore, Lovett *et al.* reported that, although pH-insensitive methyl ester-capped $PGMA_{59}$–$PHPMA_{160}$ worm gels exhibited thermoresponsive behavior at both neutral and low pH, the corresponding pH-sensitive HOOC–$PGMA_{56}$–$HPMA_{155}$ worm gel only exhibited thermoresponsive behavior when the majority of its carboxylic acid end-groups were protonated (*i.e.* below its pK_a of 4.7).[28] This is important because it provides direct evidence that anionic end-groups can prevent (or hinder) access to higher order morphologies. Alternatively, TEM studies of HOOC–$PHEA_{73}$–$PHBA_{421}$ vesicles crosslinked at 10% w/w provided evidence for the coexistence of populations of both spherical and tubular vesicles (see Fig. 9C). In principle, the latter weakly anisotropic nano-objects might account for the persistence of the Maltese cross at high PHBA DPs. Furthermore, the highly hydrated nature of the PHBA membranes may lead to some degree of elongation under applied shear (see Table S2, ESI†).

In a further set of experiments, the thermoresponsive behavior of a 20% w/w aqueous dispersion of HOOC–$PHEA_{73}$–$PHBA_{265}$ nano-objects was assessed by visual inspection at 2, 23 and 53 °C, allowing 10 min equilibration at each temperature (see Fig. 11). On cooling from 23 to 2 °C, the initial transient free-standing gel became a free-flowing fluid, see Fig. 11A(i) and 11A(ii). For other PISA systems,[41,74,88] including the closely related thermoresponsive HBA-rich nanoparticles reported by Byard *et al.*,[42] such degelation is associated with a worm-to-sphere transition (see Fig. 11B). Reheating the flowing dispersion to 23 °C resulted in reconstitution of a transient free-standing gel [Fig. 11A(iii)], suggesting that this worm-to-sphere transition is reversible. Moreover, heating to 53 °C yielded a turbid free-flowing dispersion [Fig. 11A(iv)], which is consistent with a worm-to-vesicle transition (see Fig. 11B).[42,49] This second thermal transition also appeared to be reversible on returning to 23 °C [Fig. 11A(v)].

Finally, the same 20% w/w aqueous dispersion of HOOC–$PHEA_{73}$–$PHBA_{265}$ nano-objects was studied by variable temperature oscillatory rheology at pH 7 (see Fig. 11C and D). At sub-ambient temperatures, the loss modulus (G'') exceeds the storage modulus (G'), indicating a fluid rather than a gel. However, as the complex viscosity, $|\eta^*|$, remains at about 3 Pa s, the free-flowing dispersion is still relatively viscous, see Fig. 11A(ii). As the temperature is raised, G', G'' and $|\eta^*|$ each

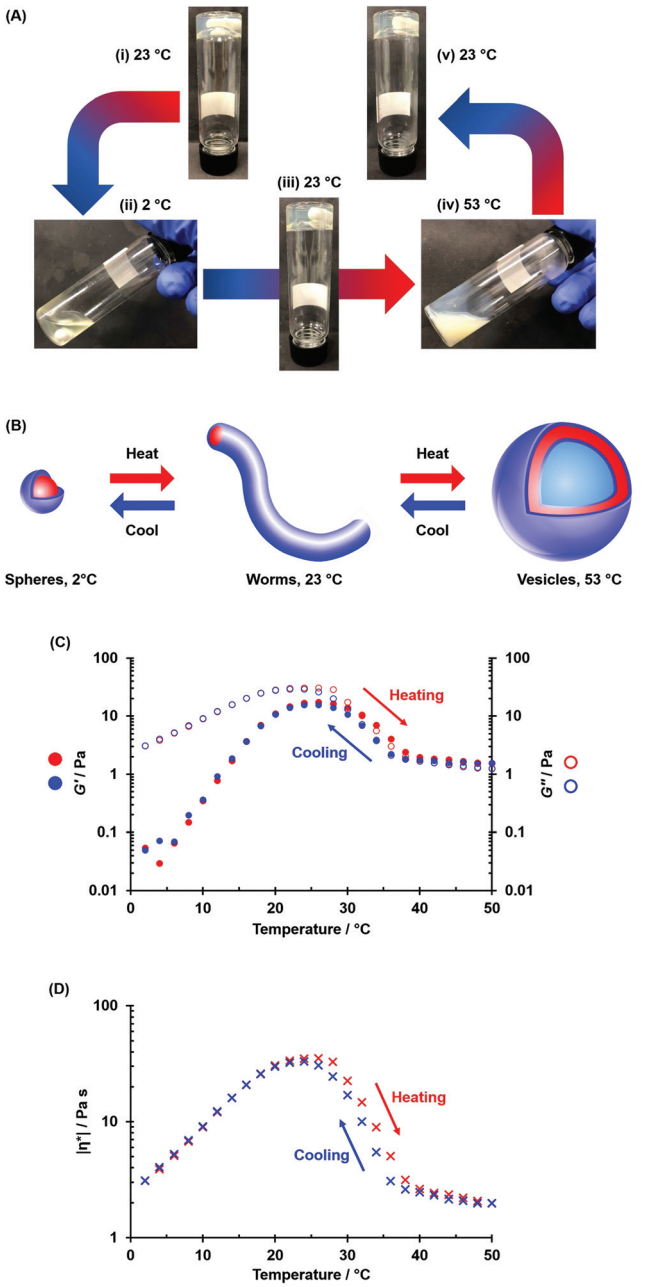

Fig. 11 (A) Digital photographs recorded for a 20% w/w aqueous dispersion of HOOC–$PHEA_{73}$–$PHBA_{265}$ nano-objects at pH 7, with 10 min equilibration being allowed at each temperature: (i) original transient free-standing gel at 23 °C; (ii) free-flowing fluid at 2 °C; (iii) reconstituted transient free-standing gel at 23 °C; (iv) turbid, free-flowing fluid at 53 °C; (v) final transient free-standing gel at 23 °C. These images are consistent with the presence of spheres (ii), worms (i), (iii) and (v) and vesicles (iv), respectively. (B) Schematic representation of the thermoreversible morphological transitions. (C and D) Variable temperature oscillatory rheology data obtained on first heating (red symbols) and then cooling (blue symbols) the same 20% w/w aqueous dispersion of HOOC–$PHEA_{73}$–$PHBA_{265}$ nano-objects at pH 7. The dispersion was equilibrated at 2 °C for 20 min prior to heating, with G' (solid symbols, C), G'' (open symbols, C) and $|\eta^*|$ (complex viscosity, crosses, D) recorded at 2 °C intervals, with 3 min being allowed for thermal equilibration at each temperature. This thermal cycle was conducted at an applied strain amplitude of 1.0% and an angular frequency of 1.0 rad s^{-1}.

pass through a maximum value at around 22–28 °C before tending towards 1 Pa and 2 Pa s, respectively, above 40 °C. Unusually, gelation occurs *after* these maxima, with CGT of 32 °C and 34 °C being observed on heating and cooling, respectively, as $|\eta^*|$ rapidly decreases. This rheology profile is similar to that reported by Byard *et al.* for a 20% w/w aqueous dispersion of HBA-rich nano-objects.[42] In this prior study, TEM studies of covalently-stabilized nano-objects that had been crosslinked at various temperatures provided confirmation of reversible sphere-to-worm and worm-to-vesicle morphological transitions between 1 and 50 °C. Furthermore, almost perfect thermoreversibility with minimal hysteresis is indicated by the rheological data shown in Fig. 11C and D, which is consistent with visual inspection [see Fig. 11A(i–v)].

Rheological studies conducted on three other HOOC–$PHEA_{73}$–$PHBA_y$ nano-objects (y = 217, 243 or 289) indicated that lower PHBA DPs lead to higher CGTs (see Fig. S9, ESI†). Similar observations were reported by Verber *et al.* for aqueous dispersions of other thermoresponsive diblock copolymer worms.[89] Notably, all gels formed by these HOOC–$PHEA_{73}$–$PHBA_y$ nano-objects were relatively weak, with maximum $|\eta^*|$ values increasing from approximately 14 to 40 Pa s with increasing PHBA DP (see Fig. 11D and Fig. S9, ESI†). Presumably, this is the result of repulsive inter-worm interactions arising from the anionic end-groups, which reduces the number of inter-worm contacts that are believed to be responsible for macroscopic gelation.[90] Similar observations were reported by Penfold and co-workers.[47,48] One reviewer of this manuscript has suggested that it would be interesting to perform further rheology studies to examine the effect of varying the solution pH on the thermoresponsive behaviour of such nano-objects. This is an interesting suggestion that warrants further consideration but unfortunately such experiments are beyond the scope of the current study.

Conclusions

The synthesis of new all-acrylic $PHEA_x$–$PHBA_y$ diblock copolymer nano-objects has been achieved *via* an efficient one-pot aqueous PISA protocol. Such nano-objects proved to be unusually sensitive to changes in pH, salt concentration, temperature and also copolymer concentration. When using a suitable carboxylic acid-functionalized RAFT agent, DLS and aqueous electrophoresis studies indicated that HOOC–$PHEA_{73}$–$PHBA_{217}$ spheres underwent reversible flocculation below pH 5.1, which corresponds to the pK_a for the carboxylic acid end-groups located on the PHEA stabilizer chains. Moreover, these nanoparticles also exhibited high salt sensitivity, with incipient flocculation occurring in the presence of 20–60 mM KCl. However, unlike the pH-dependent colloidal stability reported by Gibson *et al.* for the analogous HOOC–$PNMEP_x$–$PHPMA_y$ nanoparticles,[69] such aggregation appears to be unrelated to LCST-type behavior. Instead, the $PHEA_{73}$ stabilizer is not sufficiently long to confer effective steric stabilization so ionization of the carboxylic acid end-groups is required to confer additional colloidal stability *via electrosteric* stabilization. Furthermore, when HOOC–$PHEA_x$–$PHBA_y$ spheres were prepared using longer PHEA stabilizers (x = 105 and 140), relatively effective steric stabilization was maintained even when targeting longer PHBA DPs, as indicated by the elimination of the requirement for end-group ionization. Conversely, by switching the RAFT agent functionality from carboxylic acid to morpholine, colloidally stable Mo–$PHEA_{76}$–$PHBA_{160}$ nanoparticles could be prepared that exhibited *complementary* pH-dependent colloidal stability behavior: such dispersions remained stable at low pH but became highly flocculated above pH 5.

Discrepancies between the physical appearance of a series of HOOC–$PHEA_{73}$–$PHBA_y$ nanoparticles (where y = 104–421) prepared at 20% w/w and their corresponding DLS data obtained at 0.1% w/w suggested that such nano-objects were unstable to dilution. This unexpected instability was supported by TEM studies of HOOC–$PHEA_{73}$–$PHBA_{243}$ and HOOC–$PHEA_{73}$–$PHBA_{421}$ nanoparticles crosslinked using glutaraldehyde at either 0.1% w/w or 10–20% w/w. At 0.1% w/w, such covalent stabilization simply indicated a spherical morphology for both diblock copolymers. In contrast, worms (y = 243) or vesicles (y = 421) were observed by TEM when these formulations were crosslinked at 20% w/w or 10% w/w, respectively. Similarly, the strong Maltese cross observed in SIPLI studies of the as-synthesized 20% w/w HOOC–$PHEA_{73}$–$PHBA_{243}$ nano-objects also suggested a highly anisotropic worm morphology. Therefore, morphological assignments of spheres, a sphere/worm mixed phase, pure worms and a worm/vesicle mixed phase were made based on (i) the physical appearance of the 20% w/w dispersions and (ii) SIPLI studies conducted at the same concentration. However, TEM studies of GA-crosslinked HOOC–$PHEA_{73}$–$PHBA_{421}$ nano-objects provided evidence for a population of tubular vesicles rather than worms.

Finally, the thermoresponsive behavior of a 20% w/w aqueous dispersion of HOOC–$PHEA_{73}$–$PHBA_{265}$ nano-objects was examined at pH 7 using variable temperature oscillatory rheology. The rheological profile and corresponding visual appearance observed between 2 and 50 °C was similar to that reported by Byard *et al.* for similar thermoresponsive HBA-rich nanoparticles[42] and almost perfect thermoreversibility was obtained. This suggests that HOOC–$PHEA_{73}$–$PHBA_{265}$ forms spheres at sub-ambient temperatures, worms at around ambient temperature, and vesicles at elevated temperatures.

Conflicts of interest

There are no conflicts to declare.

Acknowledgements

We thank the EPSRC for a DTA PhD studentship to support D. L.B. S.P.A. acknowledges an EPSRC Particle Technology Fellowship grant (EP/R003009).

Notes and references

1 B. Charleux, G. Delaittre, J. Rieger and F. D'Agosto, *Macromolecules*, 2012, **45**, 6753–6765.
2 J. T. Sun, C. Y. Hong and C. Y. Pan, *Polym. Chem.*, 2013, **4**, 873–881.
3 N. J. Warren and S. P. Armes, *J. Am. Chem. Soc.*, 2014, **136**, 10174–10185.
4 J. Rieger, *Macromol. Rapid Commun.*, 2015, **36**, 1458–1471.
5 Y. Pei, A. B. Lowe and P. J. Roth, *Macromol. Rapid Commun.*, 2017, **38**, 1600528.
6 N. J. W. Penfold, J. Yeow, C. Boyer and S. P. Armes, *ACS Macro Lett.*, 2019, **8**, 1029–1054.
7 X. Wang and Z. An, *Macromol. Rapid Commun.*, 2019, **40**, 1800325.
8 F. D'Agosto, J. Rieger and M. Lansalot, *Angew. Chem., Int. Ed.*, 2020, **59**, 8368–8392.
9 I. Chaduc, W. Zhang, J. Rieger, M. Lansalot, F. D'Agosto and B. Charleux, *Macromol. Rapid Commun.*, 2011, **32**, 1270–1276.
10 A. Blanazs, J. Madsen, G. Battaglia, A. J. Ryan and S. P. Armes, *J. Am. Chem. Soc.*, 2011, **133**, 16581–16587.
11 L. A. Fielding, M. J. Derry, V. Ladmiral, J. Rosselgong, A. M. Rodrigues, L. P. D. Ratcliffe, S. Sugihara and S. P. Armes, *Chem. Sci.*, 2013, **4**, 2081–2087.
12 A. B. Lowe, *Polymer*, 2016, **106**, 161–181.
13 S. Y. Khor, N. P. Truong, J. F. Quinn, M. R. Whittaker and T. P. Davis, *ACS Macro Lett.*, 2017, **6**, 1013–1019.
14 J. Tan, J. He, X. Li, Q. Xu, C. Huang, D. Liu and L. Zhang, *Polym. Chem.*, 2017, **8**, 6853–6864.
15 J. Chiefari, Y. K. B. Chong, F. Ercole, J. Krstina, J. Jeffery, T. P. T. Le, R. T. A. Mayadunne, G. F. Meijs, C. L. Moad, G. Moad, E. Rizzardo, S. H. Thang and C. South, *Macromolecules*, 1998, **31**, 5559–5562.
16 G. Moad, E. Rizzardo and S. H. Thang, *Aust. J. Chem.*, 2005, **58**, 379–410.
17 M. R. Hill, R. N. Carmean and B. S. Sumerlin, *Macromolecules*, 2015, **48**, 5459–5469.
18 M. Benaglia, J. Chiefari, Y. K. Chong, G. Moad, E. Rizzardo and S. H. Thang, *J. Am. Chem. Soc.*, 2009, **131**, 6914–6915.
19 G. Moad and E. Rizzardo, *Polym. Int.*, 2020, **69**, 658–661.
20 J. N. Israelachvili, D. J. Mitchell and B. W. Ninham, *J. Chem. Soc., Faraday Trans. 2*, 1976, **72**, 1525–1568.
21 J. N. Israelachvili, *Intermolecular and Surface Forces*, Academic Press, London, 3rd edn, 2011.
22 A. Blanazs, S. P. Armes and A. J. Ryan, *Macromol. Rapid Commun.*, 2009, **30**, 267–277.
23 Z. An, Q. Shi, W. Tang, C. K. Tsung, C. J. Hawker and G. D. Stucky, *J. Am. Chem. Soc.*, 2007, **129**, 14493–14499.
24 S. Boissé, J. Rieger, G. Pembouong, P. Beaunier and B. Charleux, *J. Polym. Sci., Part A: Polym. Chem.*, 2011, **49**, 3346–3354.
25 A. Blanazs, A. J. Ryan and S. P. Armes, *Macromolecules*, 2012, **45**, 5099–5107.
26 W. Zhang, F. D'Agosto, O. Boyron, J. Rieger and B. Charleux, *Macromolecules*, 2012, **45**, 4075–4084.
27 M. Semsarilar, V. Ladmiral, A. Blanazs and S. P. Armes, *Langmuir*, 2012, **28**, 914–922.
28 J. R. Lovett, N. J. Warren, L. P. D. Ratcliffe, M. K. Kocik and S. P. Armes, *Angew. Chem., Int. Ed.*, 2015, **54**, 1279–1283.
29 G. Mellot, J. M. Guigner, L. Bouteiller, F. Stoffelbach and J. Rieger, *Angew. Chem., Int. Ed.*, 2019, **58**, 3173–3177.
30 W. Zhang, F. D'Agosto, P. Y. Dugas, J. Rieger and B. Charleux, *Polymer*, 2013, **54**, 2011–2019.
31 A. A. Cockram, T. J. Neal, M. J. Derry, O. O. Mykhaylyk, N. S. J. Williams, M. W. Murray, S. N. Emmett and S. P. Armes, *Macromolecules*, 2017, **50**, 796–802.
32 F. L. Hatton, A. M. Park, Y. Zhang, G. D. Fuchs, C. K. Ober and S. P. Armes, *Polym. Chem.*, 2019, **10**, 194–200.
33 E. E. Brotherton, F. L. Hatton, A. A. Cockram, M. J. Derry, A. Czajka, E. J. Cornel, P. D. Topham, O. O. Mykhaylyk and S. P. Armes, *J. Am. Chem. Soc.*, 2019, **141**, 13664–13675.
34 X. Dai, L. Yu, Y. Zhang, L. Zhang and J. Tan, *Macromolecules*, 2019, **52**, 7468–7476.
35 P. Galanopoulo, P. Y. Dugas, M. Lansalot and F. D'Agosto, *Polym. Chem.*, 2020, **11**, 3922–3930.
36 C. J. Ferguson, R. J. Hughes, D. Nguyen, B. T. T. Pham, R. G. Gilbert, A. K. Serelis, C. H. Such and B. S. Hawkett, *Macromolecules*, 2005, **38**, 2191–2204.
37 J. Rieger, W. Zhang, F. Stoffelbach and B. Charleux, *Macromolecules*, 2010, **43**, 6302–6310.
38 N. P. Truong, M. V. Dussert, M. R. Whittaker, J. F. Quinn and T. P. Davis, *Polym. Chem.*, 2015, **6**, 3865–3874.
39 S. L. Canning, V. J. Cunningham, L. P. D. Ratcliffe and S. P. Armes, *Polym. Chem.*, 2017, **8**, 4811–4821.
40 F. H. Sobotta, M. T. Kuchenbrod, C. Grune, D. Fischer, S. Hoeppener and J. C. Brendel, *Polym. Chem.*, 2021, **12**, 1668–1680.
41 J. Tan, Y. Bai, X. Zhang and L. Zhang, *Polym. Chem.*, 2016, **7**, 2372–2380.
42 S. J. Byard, C. T. O'Brien, M. J. Derry, M. Williams, O. O. Mykhaylyk, A. Blanazs and S. P. Armes, *Chem. Sci.*, 2020, **11**, 396–402.
43 F. H. Sobotta, M. Kuchenbrod, S. Hoeppener and J. C. Brendel, *Nanoscale*, 2020, **12**, 20171–20176.
44 X. Wang, J. Zhou, X. Lv, B. Zhang and Z. An, *Macromolecules*, 2017, **50**, 7222–7232.
45 N. J. Warren, M. J. Derry, O. O. Mykhaylyk, J. R. Lovett, L. P. D. Ratcliffe, V. Ladmiral, A. Blanazs, L. A. Fielding and S. P. Armes, *Macromolecules*, 2018, **51**, 8357–8371.
46 J. R. Lovett, N. J. Warren, S. P. Armes, M. J. Smallridge and R. B. Cracknell, *Macromolecules*, 2016, **49**, 1016–1025.
47 N. J. W. Penfold, J. R. Lovett, N. J. Warren, P. Verstraete, J. Smets and S. P. Armes, *Polym. Chem.*, 2016, **7**, 79–88.
48 N. J. W. Penfold, J. R. Lovett, P. Verstraete, J. Smets and S. P. Armes, *Polym. Chem.*, 2017, **8**, 272–282.
49 L. P. D. Ratcliffe, M. J. Derry, A. Ianiro, R. Tuinier and S. P. Armes, *Angew. Chem., Int. Ed.*, 2019, **58**, 18964–18970.
50 O. J. Deane, J. Jennings and S. P. Armes, *Chem. Sci.*, 2021, **12**, 13719–13729.
51 L. Zhang, K. Katapodi, T. P. Davis, C. Barner-Kowollik and M. H. Stenzel, *J. Polym. Sci., Part A: Polym. Chem.*, 2006, **44**, 2177–2194.

52 Y. Chan, T. Wong, F. Byrne, M. Kavallaris and V. Bulmus, *Biomacromolecules*, 2008, **9**, 1826–1836.
53 C. D. Vo, J. Rosselgong, S. P. Armes and N. Tirelli, *J. Polym. Sci., Part A: Polym. Chem.*, 2010, **48**, 2032–2043.
54 H. Mori and H. Tanaka, *Macromol. Chem. Phys.*, 2011, **212**, 2349–2359.
55 W. Steinhauer, R. Hoogenboom, H. Keul and M. Moeller, *Macromolecules*, 2013, **46**, 1447–1460.
56 B. Louage, Q. Zhang, N. Vanparijs, L. Voorhaar, S. Vande Casteele, Y. Shi, W. E. Hennink, J. Van Bocxlaer, R. Hoogenboom and B. G. De Geest, *Biomacromolecules*, 2015, **16**, 336–350.
57 M. Lu, Y. Y. Khine, F. Chen, C. Cao, C. J. Garvey, H. Lu and M. H. Stenzel, *Biomacromolecules*, 2019, **20**, 273–284.
58 J. Zhou, W. Zhang, C. Hong and C. Y. Pan, *Polym. Chem.*, 2016, **7**, 3259–3267.
59 V. Tkachenko, C. Matei Ghimbeu, C. Vaulot, L. Vidal, J. Poly and A. Chemtob, *Polym. Chem.*, 2019, **10**, 2316–2326.
60 J. Tan, Y. Peng, D. Liu, C. Huang, M. Yu, D. Jiang and L. Zhang, *Macromol. Chem. Phys.*, 2016, **217**, 1723–1728.
61 W. Steinhauer, R. Hoogenboom, H. Keul and M. Moeller, *Macromolecules*, 2010, **43**, 7041–7047.
62 J. T. Lai, D. Filla and R. Shea, *Macromolecules*, 2002, **35**, 6754–6756.
63 R. Chapman, G. G. Warr, S. Perrier and K. A. Jolliffe, *Chem. – Eur. J.*, 2013, **19**, 1955–1961.
64 P. E. Millard, L. Barner, J. Reinhardt, M. R. Buchmeiser, C. Barner-Kowollik and A. H. E. Müller, *Polymer*, 2010, **51**, 4319–4328.
65 L. Martin, G. Gody and S. Perrier, *Polym. Chem.*, 2015, **6**, 4875–4886.
66 T. Junkers and C. Barner-Kowollik, *J. Polym. Sci., Part A: Polym. Chem.*, 2008, **46**, 7585–7605.
67 Y. Li and S. P. Armes, *Angew. Chem., Int. Ed.*, 2010, **49**, 4042–4046.
68 I. Bannister, N. C. Billingham, S. P. Armes, S. P. Rannard and P. Findlay, *Macromolecules*, 2006, **39**, 7483–7492.
69 R. R. Gibson, S. P. Armes, O. M. Musa and A. Fernyhough, *Polym. Chem.*, 2019, **10**, 1312–1323.
70 G. Vancoillie, D. Frank and R. Hoogenboom, *Prog. Polym. Sci.*, 2014, **39**, 1074–1095.
71 M. B. Einarson and J. C. Berg, *J. Colloid Interface Sci.*, 1993, **155**, 165–172.
72 M. Save, M. Manguian, C. Chassenieux and B. Charleux, *Macromolecules*, 2005, **38**, 280–289.
73 L. P. D. Ratcliffe, B. E. McKenzie, G. M. D. Le Bouëdec, C. N. Williams, S. L. Brown and S. P. Armes, *Macromolecules*, 2015, **48**, 8594–8607.
74 A. Blanazs, R. Verber, O. O. Mykhaylyk, A. J. Ryan, J. Z. Heath, C. W. I. Douglas and S. P. Armes, *J. Am. Chem. Soc.*, 2012, **134**, 9741–9748.
75 B. Akpinar, L. A. Fielding, V. J. Cunningham, Y. Ning, O. O. Mykhaylyk, P. W. Fowler and S. P. Armes, *Macromolecules*, 2016, **49**, 5160–5171.
76 V. J. Cunningham, A. M. Alswieleh, K. L. Thompson, M. Williams, G. J. Leggett, S. P. Armes and O. M. Musa, *Macromolecules*, 2014, **47**, 5613–5623.
77 M. Williams, N. J. W. Penfold and S. P. Armes, *Polym. Chem.*, 2016, **7**, 384–393.
78 M. Chenal, L. Bouteiller and J. Rieger, *Polym. Chem.*, 2013, **4**, 752–762.
79 G. Liu, Q. Qiu and Z. An, *Polym. Chem.*, 2012, **3**, 504–513.
80 J. Bang, S. Jain, Z. Li, T. P. Lodge, J. S. Pedersen, E. Kesselman and Y. Talmon, *Macromolecules*, 2006, **39**, 1199–1208.
81 A. Czajka and S. P. Armes, *Chem. Sci.*, 2020, **11**, 11443–11454.
82 C. Cao, F. Chen, C. J. Garvey and M. H. Stenzel, *ACS Appl. Mater. Interfaces*, 2020, **12**, 30221–30233.
83 O. J. Deane, J. Jennings, T. J. Neal, O. M. Musa, A. Fernyhough and S. P. Armes, *Chem. Mater.*, 2021, **33**, 7767–7779.
84 O. O. Mykhaylyk, N. J. Warren, A. J. Parnell, G. Pfeifer and J. Laeuger, *J. Polym. Sci., Part B: Polym. Phys.*, 2016, **54**, 2151–2170.
85 O. O. Mykhaylyk, *Soft Matter*, 2010, **6**, 4430–4440.
86 J. Tan, H. Sun, M. Yu, B. S. Sumerlin and L. Zhang, *ACS Macro Lett.*, 2015, **4**, 1249–1253.
87 M. Semsarilar, V. Ladmiral, A. Blanazs and S. P. Armes, *Langmuir*, 2013, **29**, 7416–7424.
88 Y. Pei, N. C. Dharsana, J. A. Van Hensbergen, R. P. Burford, P. J. Roth and A. B. Lowe, *Soft Matter*, 2014, **10**, 5787–5796.
89 R. Verber, A. Blanazs and S. P. Armes, *Soft Matter*, 2012, **8**, 9915–9922.
90 J. R. Lovett, M. J. Derry, P. Yang, F. L. Hatton, N. J. Warren, P. W. Fowler and S. P. Armes, *Chem. Sci.*, 2018, **9**, 7138–7144.